Tanja Scholz, Florian Pielnhofer, Roland Eger and Bettina V. Lotsch*

Lanthanide orthothiophosphates revisited: single-crystal X-ray, Raman, and DFT studies of $TmPS_4$ and $YbPS_4$

https://doi.org/10.1515/znb-2019-0217
Received December 12, 2019; accepted December 20, 2019

Abstract: The crystal structures of the lanthanide orthothiophosphates $LnPS_4$ (Ln = lanthanide) have been extensively investigated in the past. Up to now, however, single crystals of two members of this series – $TmPS_4$ and $YbPS_4$ – have not been available. Here, we report a modified synthesis protocol for $TmPS_4$ and $YbPS_4$ yielding single crystals suitable for X-ray diffraction. Both compounds crystallize in the tetragonal space group $I4_1/acd$ (no. 142) with 16 formula units per unit cell and adopt the $SmPS_4$ parent structure, like most reported lanthanide orthothiophosphates. The structures contain isolated $[PS_4]^{3-}$ tetrahedra and two crystallographically independent Ln^{3+} cations, which form trigonal-dodecahedral $[LnS_8]^{13-}$ polyhedra. The lattice parameters for $TmPS_4$ are $a = 10.598(2)$, $c = 18.877(4)$ Å with $V = 2120.2(6)$ Å^3, and for $YbPS_4$ $a = 10.577(2)$, $c = 18.827(4)$ Å with $V = 2106.2(7)$ Å^3. The DFT-calculated electronic band structures indicate semiconducting behavior and reveal indirect band gaps of 2.1–2.2 eV, consistent with the reddish brown color of $YbPS_4$, but underestimating the band gap of pale-yellow $TmPS_4$. The Raman spectra are dominated by $[PS_4]^{3-}$ vibrations as confirmed by DFT-calculated phonon spectra. DTA measurements reveal remarkably high thermal stability compared to other known orthothiophosphate compounds.

Keywords: electronic band structure; orthothiophosphates; phonon spectra; Raman spectroscopy; rare earth elements; single-crystal X-ray diffraction; thermal stability.

***Corresponding author: Bettina V. Lotsch,** Nanochemistry Department, Max Planck Institute for Solid State Research, Heisenbergstraße 1, 70569 Stuttgart, Germany; Department of Chemistry, Ludwig-Maximilians-Universität München, Butenandtstraße 5–13, 81377 München, Germany; and Cluster of Excellence E-conversion and Center for Nanoscience, Schellingstraße 4, 80799 München, Germany, e-mail: b.lotsch@fkf.mpg.de
Tanja Scholz and Roland Eger: Nanochemistry Department, Max Planck Institute for Solid State Research, Heisenbergstraße 1, 70569 Stuttgart, Germany
Florian Pielnhofer: Nanochemistry Department, Max Planck Institute for Solid State Research, Heisenbergstraße 1, 70569 Stuttgart, Germany; and new address: University of Regensburg, Institute of Inorganic Chemistry, Universitätsstraße 31, 93040 Regensburg, Germany

Dedicated to: Professor Arndt Simon on the occasion of his 80th birthday.

1 Introduction

A multitude of ternary compounds based on the orthothiophosphate anion $[PS_4]^{3-}$ has been reported over the last decades, and they continue to receive significant attention owing to their varied materials properties, even more than 125 years after their discovery [1–11]. The first compound, $SbPS_4$, was reported by Glatzel in 1891 [12], followed 2 years later by a comprehensive study on "Normale Sulfophosphate", describing their properties and syntheses [13]. However, the crystal structure of $SbPS_4$ remained unknown until 2006, when Malliakas and Kanatzidis reported that this compound naturally forms single walled nanotubes with an outer diameter of 13 Å and an overall hexagonal close packing of the tubes [14].

The trivalent orthothiophosphates show a large structural variety which is realized by linking different types of polyhedra. Recent reports on superionic conductivities found in the alkali metal orthothiophosphates has established these compounds as promising solid electrolytes for all-solid-state batteries (e.g. β-Li_3PS_4 [15], Na_3PS_4 [16]). Additionally, they are studied as materials for next-generation digital electronics due to antiferromagnetic semiconducting properties in some layered compounds (e.g. $CrPS_4$ [17]). Interest in this family of compounds increased further when first principles and experimental investigations showed their potential for applications in nonlinear optics, in particular for mid infrared coherent light generation [18].

Lanthanide orthothiophosphates $LnPS_4$ (Ln = lanthanide) [6] are, with few exceptions, isostructural to the archetypical $SmPS_4$ [11] that features three-dimensional connectivity and crystallizes in the tetragonal space group $I4_1/acd$ (no. 142). They all contain slightly disordered, discrete $[PS_4]^{3-}$ tetrahedra, and the two crystallographically different Ln^{3+} cations are eight-fold coordinated by

sulphur atoms, $[LnS_8]^{13-}$. The two candidates that fall out of line are $LuPS_4$ [4] and $ScPS_4$ [7]. Both exceptions are layered compounds with van der Waals gaps between the $LnPS_4$ sheets. Although $ScPS_4$ is reported to crystallize in the triclinic space group $P\bar{1}$ (no. 2) and $LuPS_4$ crystallizes in the monoclinic space group $P2_1/n$ (no. 14), their structures are similar: The cations Sc^{3+} and Lu^{3+} are seven-fold coordinated by sulphur atoms, $[LnS_7]^{11-}$, and contain isolated $[PS_4]^{3-}$ tetrahedra. Furthermore, $LuPS_4$ is the only diamagnetic member of the lanthanide series. The only missing member is "$EuPS_4$", probably due to the fact that the divalent compound $Eu_2P_2S_6$ is more stable and, therefore, formed preferentially during the synthetic attempts [6, 19].

During our investigations on lanthanide orthothiophosphates we noticed that $TmPS_4$ and $YbPS_4$ have not been synthesized as single crystals [6], even though their lattice parameters were reported from X-ray powder diffraction experiments several times [8, 20–22]. For $TmPS_4$, Huang et al. [21] arrived at lattice parameters of $a = 10.5962(2)$, $c = 18.881(1)$ Å, and Wibbelmann et al. [5] described a brownish color (contrary to the pale-yellow color of the compound presented here). For $YbPS_4$, different lattice parameters were reported in the literature, namely $a = 10.571(1)$, $c = 18.817(2)$ Å in a study by Le Rolland et al. [8], which are significantly smaller than the powder lattice parameters $a = 10.664(2)$, $c = 18.989(4)$ Å reported by Palkina et al. [6, 22]. Further, Le Rolland et al. described the color of $YbPS_4$ to be black, while we will show that the color is reddish brown [8].

In this publication, we report a new synthesis protocol for $TmPS_4$ and $YbPS_4$, by which we were able to obtain single crystals suitable for structure elucidation. $TmPS_4$ and $YbPS_4$ were further characterized by Raman spectroscopy supported by quantum chemical calculations, evidencing the presence of the $[PS_4]^{3-}$ unit. Further, we demonstrate an exceptionally high thermal stability of both compounds as determined by differential thermal analysis (DTA).

2 Results and discussion

2.1 Syntheses of $TmPS_4$ and $YbPS_4$

$TmPS_4$ and $YbPS_4$ were synthesized in a solid state reaction from the respective rare earth metals, P_4S_{10} and sulphur at elevated temperatures. Both compounds form crystals roughly 100 µm in size. $TmPS_4$ was obtained as pale-yellow, transparent, columnar crystals (Fig. 1) on the surface of the Tm metal, contrary to Wibbelmann and Brockner's description of the color being brownish [5]. Single crystals of $YbPS_4$ appear dark red in color if large (ca. 100 µm) and well-shaped, reddish brown yet transparent if thin (Fig. 1). We did not observe the black color that was described previously by Le Rolland et al. [8].

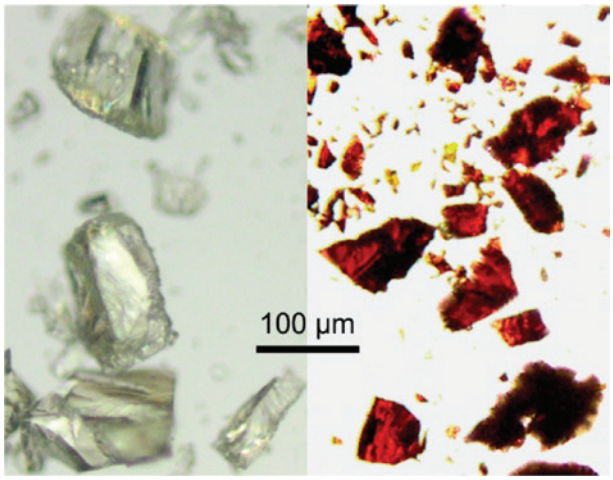

Fig. 1: Pale-yellow crystals of $TmPS_4$ (left) and dark, reddish brown crystals of $YbPS_4$ (right).

2.2 Structures of $TmPS_4$ and $YbPS_4$

The crystal structures of $TmPS_4$ and $YbPS_4$ were investigated by single-crystal X-ray diffraction. Both compounds crystallize in the tetragonal space group $I4_1/acd$ (no. 142) with sixteen formula units per unit cell, and are isostructural to $SmPS_4$ [11] (*cf.* Tables 1, S1, S2, Supporting Information available online). The structure contains isolated $[PS_4]^{3-}$ tetrahedra that are slightly distorted (Fig. 2a) and two crystallographically independent Ln^{3+} cations (Wyckoff positions 8*a* and 8*b*). The Ln^{3+} cations are eight-fold coordinated by sulphur atoms (trigonal dodecahedral $[LnS_8]^{13-}$ polyhedra) and each cation is coordinated by four $[PS_4]^{3-}$ tetrahedra (Fig. 2b).

The lattice parameters of $TmPS_4$ are $a = 10.598(2)$, $c = 18.877(4)$ Å with $V = 2120.2(6)$ Å^3 and agree well with the ones reported by Huang et al. ($a = 10.5962(2)$, $c = 18.881(1)$ Å) [21] which were determined by powder X-ray diffraction. We determined the lattice parameters of $YbPS_4$ to be $a = 10.577(2)$, $c = 18.827(4)$ Å with $V = 2106.2(7)$ Å^3. They are consistent with the powder lattice parameters reported by Le Rolland et al. ($a = 10.571(1)$, $c = 18.817(2)$ Å) [8], but significantly smaller than the powder lattice parameters reported by Palkina et al. ($a = 10.664(2)$, $c = 18.989(4)$ Å) [6, 22]. Based on their 2004 study [9], Schleid et al.

Table 1: Crystallographic data of $TmPS_4$ and $YbPS_4$ as obtained from single-crystal X-ray diffraction (Mo$K\alpha$ radiation) at $T = 298$ K.

	$TmPS_4$	$YbPS_4$
Crystal shape	Column	Polyhedron
Crystal color	Pale-yellow transparent	Reddish brown transparent
Diffraction method	Single crystal	Single crystal
Radiation	Mo$K\alpha$	Mo$K\alpha$
Crystal symmetry	Tetragonal	Tetragonal
Space group	$I4_1/acd$ (no. 142)	$I4_1/acd$ (no. 142)
Lattice parameters		
$a = b$, Å	10.598(2)	10.577(2)
c, Å	18.877(4)	18.827(4)
Cell volume, Å^3	2120.2(6)	2106.2(6)
Cell content Z	16	16
2θ range, °	$6.49 \le 2\theta \le 58.38$	$6.96 \le 2\theta \le 58.46$
Index range	$-14 \le h \le 14$	$-14 \le h \le 14$
	$-14 \le k \le 14$	$-13 \le k \le 14$
	$-25 \le l \le 25$	$-24 \le l \le 24$
Total reflections	9010	9225
Unique reflections/R_{int}	728/0.1154	711/0.0825
Refined parameters	30	30
R_1/wR_2 ($F_o^2 > 4\,\sigma(F_o^2)$)	0.0258/0.0526	0.0246/0.0551
GooF	0.832	0.972
Res. electron dens. (max/min), e Å^{-3}	1.32/ – 1.37	1.24/ – 1.88
Deposition no.	CSD-1972308	CSD-1972309

For atomic coordinates and equivalent isotropic displacement factors please refer to Tables S1 and S2 (Supporting Information).

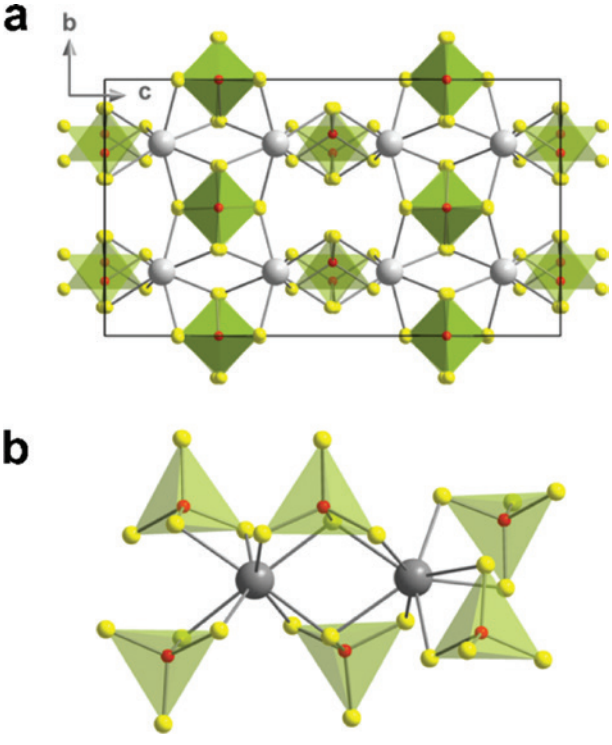

Fig. 2: (a) Crystal structure of $TmPS_4$ and $YbPS_4$ (a axis is the vertical axis, Tm/Yb atoms in grey, P atoms in red, S atoms in yellow, and isolated $[PS_4]^{3-}$ tetrahedra in green). (b) Coordination environment of the two crystallographically different Ln^{3+} cations.

rationalized in Ref. [6] this apparent inconsistency by the assumption that the compound reported as "$YbPS_4$" may in fact have been YPS_4, which would match the expected trends in the structural parameters within the lanthanide orthothiophosphate series.

In $TmPS_4$, the Tm–S bond lengths of the $[TmS_8]$ polyhedra are 2.767(2)–2.994(2) Å and the P–S bond lengths of the slightly distorted $[PS_4]^{3-}$ tetrahedra are 2.027(1)–2.033(2) Å with S–P–S angles of 106.23(7)–116.7(1)°. In $YbPS_4$, the Yb–S bond lengths of the $[YbS_8]$ polyhedra amount to 2.753(1)–2.840(1) Å and the P–S bond lengths of the slightly distorted $[PS_4]^{3-}$ tetrahedra vary between 2.0265(2) and 2.0326(2) Å with S–P–S angles between 106.15(1) and 116.75(1)°. These bond lengths and angles agree well with those of the isostructural $LnPS_4$ compounds (Ln = La–Nd, Sm, Gd–Er) [6].

To gain further insights into the electronic structure, we calculated the band structures based on density functional theory (DFT). Figure 3 exemplarily shows the electronic band structure of $YbPS_4$, confirming its semiconducting properties (*cf.* Fig. S1 for $TmPS_4$; Supporting Information). The band gap is indirect with the valence band maximum found at the Z point and the conduction band minimum located near the Σ_1 point. The indirect band gap was calculated with the dedicated *meta*-GGA potential SCAN for higher accuracy [23] resulting in

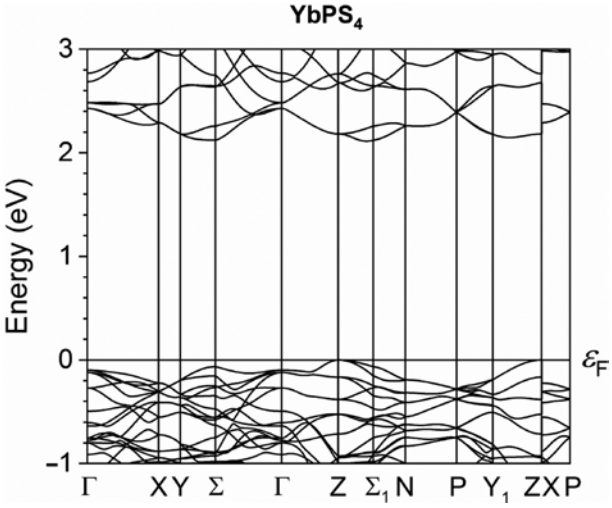

Fig. 3: Calculated electronic band structure of $YbPS_4$ with an indirect band gap of 2.11 eV.

2.11 eV, which is in good agreement with the red color of $YbPS_4$.

2.3 Raman spectroscopy

Raman spectroscopy was performed on single crystals of $TmPS_4$ and $YbPS_4$ to investigate the local bonding situation. The Raman spectra of the isostructural compounds are almost identical (*cf.* Fig. 4) and are dominated by the vibrations of the $[PS_4]^{3-}$ anion which would have T_d symmetry in the "free gas phase", but this symmetry is reduced to C_1 due to slight distortions of the tetrahedral anion in the crystal structure. The strongest bands around 430 cm^{-1} stem from vibrations that derive from the ν_1 symmetric stretching vibrations of the T_d symmetric $[PS_4]^{3-}$ anion, while the less pronounced ν_3 asymmetric stretching vibrations are split into several bands around 600 cm^{-1}. The signals in the 200 – 300 cm^{-1} region can be attributed to the ν_2 symmetric and ν_4 asymmetric bending modes of tetrahedral $[PS_4]^{3-}$. These characteristic vibrations and splittings are found in all isostructural $LnPS_4$ compounds (Ln = La–Nd, Sm, Gd–Er) [5, 8, 11, 20].

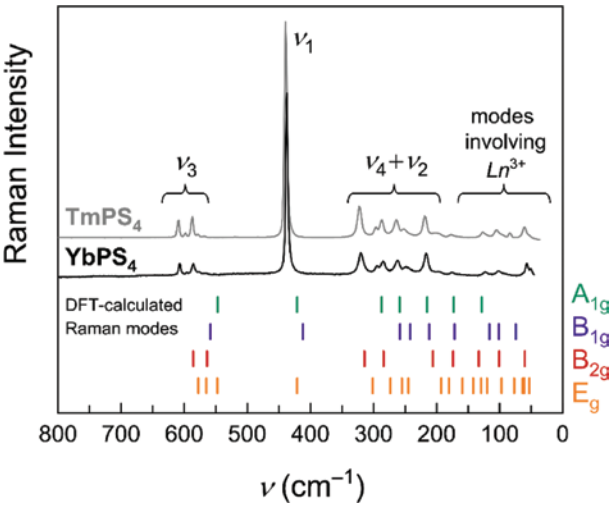

Fig. 4: Raman spectra of $TmPS_4$ and $YbPS_4$ with DFT-calculated Raman-active modes and assigned vibrational modes of the $[PS_4]^{3-}$ anion (*cf.* text).

To further interpret the Raman spectra, we simulated the density of phonon modes (IR- and Raman-active modes) of $TmPS_4$ and $YbPS_4$ by DFT, which are both found essentially identical (*cf.* Fig. S2; Supporting Information). Raman-active modes for $LnPS_4$ in space group $I4_1/acd$ (no. 142) have the irreducible representations $\Gamma_{Raman} = 7\ A_{1g} + 9\ B_{1g} + 9\ B_{2g} + 19\ E_g$ and are marked in Fig. 4. The theoretical peak positions are slightly shifted to lower wave numbers but correspond well with the experimental Raman spectra. The visualized theoretical vibrational modes confirm the above assigned $[PS_4]^{3-}$ vibrations.

2.4 Thermal behavior

The thermal behavior of $TmPS_4$ and $YbPS_4$ was studied by differential thermal analysis (DTA) measurements. $TmPS_4$ and $YbPS_4$ melt congruently. Upon heating we observed only one endothermic peak for both lanthanides, namely, at T = 1363 K for $TmPS_4$ and at 1305 K for $YbPS_4$. Upon cooling, $TmPS_4$ solidifies at 1353 K while $YbPS_4$ was slightly subcooled to 1278 K. Comparison with the thermal behavior of other orthothiophosphates studied previously suggests that $TmPS_4$ and $YbPS_4$ have a particularly high thermal stability: For example, K_2AuPS_4 and Tl_2AuPS_4 melt congruently already around 660–690 K [24], BPS_4 melts congruently at 780 K [3], and Ag_3PS_4 melts incongruently at 800 K [25]. High melting points are also found in ht-$AlPS_4$ (1070 K) [2] and Cu_3PS_4 (1240 K) [26]. Note that melting points of other lanthanide family members $LnPS_4$ are unknown.

3 Conclusions

The orthothiophosphates $TmPS_4$ and $YbPS_4$ were synthesized as single crystals of pale-yellow and reddish brown color, respectively. Single-crystal X-ray structure analyses have confirmed the two compounds to be isostructural and to adopt the well-known $SmPS_4$ structure type featuring two crystallographically independent Ln^{3+} cations that are each coordinated by four slightly distorted

$[PS_4]^{3-}$ tetrahedra. Both compounds are semiconductors with indirect band gaps calculated by DFT to be 2.1–2.2 eV, which explains the dark red color of $YbPS_4$, but fails to interpret the pale-yellow color of $TmPS_4$. The Raman spectra are dominated by the vibrations of the $[PS_4]^{3-}$ anion, as confirmed with phonon calculations. $TmPS_4$ and $YbPS_4$ show a remarkably high thermal stability with melting points above $T = 1300$ K.

4 Experimental section

4.1 Syntheses

All preparations and manipulations were carried out in a drybox under argon atmosphere. For the solid state reactions $4\ Ln\ (\mathrm{Tm;\ Yb}) + P_4S_{10} + 6\ S \rightarrow 4\ LnPS_4$ stoichiometric proportions of Tm or Yb (Johnson Matthey, pieces, distilled dendritic, 99.99%), P_4S_{10} (Acros, 98+%) and S (Alfa Aesar, 99.5%) were intimately mixed and heated in vacuum-sealed uncoated quartz tubes (length: 150 mm, inside diameter: 9 mm). $TmPS_4$ and $YbPS_4$ are both moisture sensitive and must be stored and handled under inert conditions. In order to prevent damaging of the sealed quartz tube by the initially strong exothermic reaction, the starting material was placed into a small quartz container (length: 80 mm, outer diameter: 8 mm) prior to transferring it to the quartz tube. This crucible was fused with the outer ampoule *via* melting before the entire ampoule was sealed under vacuum and water cooling.

4.1.1 Synthesis of $TmPS_4$

The stoichiometric mixture was heated up (100 K h^{-1}) to $T = 1073$ K and kept at that temperature for 2 days. Afterwards the ampoule was cooled down (25 K h^{-1}) and annealed first for 2 days at 973 K and then for another 2 days at 773 K. Subsequently, the furnace was switched off and the ampoule was removed from the furnace at room temperature. The quartz tube contained pale-yellow transparent crystals on the surface of the Tm metal. Caution: Heating above 1123 K led to an explosion of the evacuated quartz ampoule.

4.1.2 Synthesis of $YbPS_4$

A stoichiometric mixture of Yb, S, and P_4S_{10} was sealed in an evacuated quartz tube, heated up (100 K h^{-1}) to $T = 1173$ K and kept at that temperature for 1 h. Afterwards the ampoule was cooled down (25 K h^{-1}) and annealed first at 1073 K and then at 673 K for 2 days. The furnace was then switched off and the ampoule was removed from the furnace at room temperature. Dark red and well-shaped crystals of $YbPS_4$ (note: thin plates or grinded powders look reddish brown) were obtained at the bottom of the ampoule.

4.2 EDX analyses

Several single crystals were mounted on carbon tape and measured with a Tescan SEM (Vega TS 5130 MM) equipped with a SDD (silicon drift detector, Oxford) confirming the composition of the single crystals ($TmPS_4$: 16(1) at.% Tm, 17(1) at.% P, 67(1) at.% S; $YbPS_4$: 17(2) at.% Yb, 18(1) at.% P, 65(2) at.% S).

4.3 X-ray diffraction

Powder X-ray diffraction patterns of $TmPS_4$ and $YbPS_4$ were measured in sealed glass capillaries using a STOE StadiP diffractometer working with Ge-monochromated Mo$K\alpha$ radiation in Debye-Scherrer geometry. $TmPS_4$ and $YbPS_4$ single crystals suitable for X-ray diffraction were picked under a microscope in dried petroleum and mounted into sealed glass capillaries. The data collection was performed with a STOE IPDS II working with graphite-monochromated Mo$K\alpha$ radiation. For the integration of the reflection intensities and the calculation of the reciprocal lattice planes, the STOE X-Area 1.56 software was used. The structure was solved with Direct Methods and refined by least-squares fitting using the program Shelxtl [27].

Crystallographic data for the structures reported in this paper have been deposited with the Cambridge Crystallographic Data Centre, CCDC, 12 Union Road, Cambridge, CB2 1EZ, UK. Copies of the data can be obtained free of charge on quoting the depository numbers CSD-1972308 ($TmPS_4$) and CSD-1972309 ($YbPS_4$) (Fax: +44-1223-336-033; E-Mail: deposit@ccdc.cam.ac.uk, http://www.ccdc.cam.ac.uk).

4.4 Raman spectroscopy

Single crystals were selected under a microscope in dried petroleum, mounted into glass capillaries and sealed under inert atmosphere. The Raman spectra were recorded with a Jobin Yvon Typ V 010 labram single grating spectrometer, equipped with a double super razor edge filter and

a Peltier cooled CCD camera. The resolution of the spectrometer (grating 1800 $L \cdot mm^{-1}$) is 1 cm^{-1}.

4.5 DTA measurements

DTA measurements were performed under inert atmosphere in sealed quartz containers with home-built equipment described in Ref. [2]. After thermal analysis, the products were again characterized by XRD and SEM-EDX analysis.

4.6 Calculations

The electronic band structure calculations were carried out with the Vienna *Ab initio* Simulation Package (VASP) [28–30] based on density functional theory using projector-augmented-wave (PAW) potentials [31, 32] for core and valence electron separation. Exchange and correlation contributions were treated with the generalized gradient approximation as parametrized by Perdew, Burke, and Ernzerhof (GGA-PBE) [33]. Pseudopotentials for Tm and Yb were chosen that treat the 4*f* electrons as part of the atomic core. The Monkhorst-Pack [34] *k*-point mesh used for Brillouin zone integration was energetically converged for all calculations while the energy-cutoff was set to 500 eV. The convergence criterion of the electronic structure calculations was set to 10^{-7} eV. For higher accuracy, the compounds' band structures were calculated with the SCAN *meta*-GGA potential [23]. The density of phonon states were derived using the direct method [35], as implemented in Phonopy [36, 37].

5 Supporting information

Atomic coordinates and equivalent isotropic displacement factors are given as supplementary information available online (Tables S1, S2). Further, the electronic band structure as well as DFT-calculated density of phonon states of $TmPS_4$ are illustrated in Figs. S1 and S2 (DOI: 10.1515/znb-2019-0217).

Acknowledgment: The authors acknowledge financial support by the BMBF (3XP0177B (FestBatt), the Max Planck Society, and the Center for Nanoscience (CeNS). We thank *V. Duppel* for taking images of the crystals and for SEM-EDX analyses, *A. Schulz* for performing the single-crystal Raman spectroscopy, *W. Hölle* for single-crystal X-ray diffraction measurements and the Computer Service group at MPI-FKF for providing computational facilities.

References

[1] A. Simon, K. Peters, E. M. Peters, H. Hahn, *Z. Naturforsch.* **1983**, *38b*, 426–427.
[2] A. Kuhn, R. Eger, P. Ganter, V. Duppel, J. Nuss, B. V. Lotsch, *Z. Anorg. Allg. Chem.* **2014**, *640*, 2663–2668.
[3] F. Pielnhofer, L. M. Schoop, A. Kuhn, R. Eger, J. Nuss, H. Nuss, B. V. Lotsch, *Z. Anorg. Allg. Chem.* **2019**, *645*, 267–271.
[4] D. A. Cleary, B. Twamley, *Inorg. Chim. Acta* **2003**, *353*, 183–186.
[5] C. Wibbelmann, W. Brockner, B. Eisenmann, H. Schäfer, *Z. Naturforsch.* **1984**, *39a*, 190–194.
[6] T. Komm, D. Gudat, T. Schleid, *Z. Naturforsch.* **2006**, *61b*, 766–774.
[7] S. Lee, R. J. Hilt, *J. Alloys Compd.* **1992**, *189*, 269–271.
[8] B. Le Rolland, P. McMillan, P. Molinie, P. Colombet, *Eur. J. Solid State Inorg. Chem.* **1990**, *27*, 715–724.
[9] T. Komm, T. Schleid, *Z. Anorg. Allg. Chem.* **2004**, *630*, 1544–1546.
[10] K. K. Palkina, S. I. Maksimova, N. T. Chibiskova, T. B. Kuvshinova, A. N. Volodina, *Inorg. Mater.* **1984**, *20*, 1338–1341.
[11] M. Gjikaj, Habilitation thesis, University Clausthal, Clausthal, **2008**.
[12] E. Glatzel, *Ber. Dtsch. Chem. Ges.* **1891**, *24*, 3886–3888.
[13] E. Glatzel, *Z. Anorg. Allg. Chem.* **1893**, *4*, 186–226.
[14] C. D. Malliakas, M. G. Kanatzidis, *J. Am. Chem. Soc.* **2006**, *128*, 6538–6539.
[15] Z. Liu, W. Fu, E. A. Payzant, X. Yu, Z. Wu, N. J. Dudney, J. Kiggans, K. Hong, A. J. Rondinone, C. Liang, *J. Am. Chem. Soc.* **2013**, *135*, 975–978.
[16] M. Jansen, U. Henseler, *J. Solid State Chem.* **1992**, *99*, 110–119.
[17] J. Lee, T. Y. Ko, J. H. Kim, H. Bark, B. Kang, S.-G. Jung, T. Park, Z. Lee, S. Ryu, C. Lee, *ACS Nano* **2017**, *11*, 10935–10944.
[18] L. Kang, M. Zhou, J. Yao, Z. Lin, Y. Wu, C. Chen, *J. Am. Chem. Soc.* **2015**, *137*, 13049–13059.
[19] W. Broekner, R. Becker, *Z. Naturforsch.* **1987**, *42b*, 511–512.
[20] Z. Huang, V. Cajipe, P. Molinié, *J. Rare Earths* **1998**, *16*, 167–171.
[21] Z. Huang, V. Cajipe, P. Molinié, *J. Rare Earths* **1999**, *17*, 6–11.
[22] K. K. Palkina, T. B. T.B. Kuvshinova, S. I. Maksimova, N. T. Chibiskova, *Izv. Akad. Nauk SSSR Neorg. Mater.* **1998**, *25*, 1555–1556.
[23] J. Sun, A. Ruzsinszky, J. P. Perdew, *Phys. Rev. Lett.* **2015**, *115*, 036402.
[24] S. Löken, W. Tremel, *Eur. J. Inorg. Chem.* **1998**, *1998*, 283–289.
[25] H. Andrae, R. Blachnik, *J. Therm. Anal.* **1989**, *35*, 595–607.
[26] R. Blachnik, B. Gather, E. Andrae, *J. Therm. Anal.* **1991**, *37*, 1289–1298.
[27] G. M. Sheldrick, *Acta Crystallogr.* **2008**, *A64*, 112–122.
[28] S. H. Liu, *Phys. Rev. B* **1977**, *15*, 4281–4287.
[29] G. Kresse, J. Furthmüller, *Comput. Mater. Sci.* **1996**, *6*, 15–50.
[30] G. Kresse, J. Hafner, *Phys. Rev. B* **1993**, *47*, 558–561.
[31] P. E. Blöchl, *Phys. Rev. B* **1994**, *50*, 17953–17979.

[32] G. Kresse, D. Joubert, *Phys. Rev. B* **1999**, *59*, 1758–1775.
[33] J. P. Perdew, K. Burke, M. Ernzerhof, *Phys. Rev. Lett.* **1996**, *77*, 3865–3868.
[34] H. J. Monkhorst, J. D. Pack, *Phys. Rev. B* **1976**, *13*, 5188–5192.
[35] K. Parlinski, Z. Q. Li, Y. Kawazoe, *Phys. Rev. Lett.* **1997**, *78*, 4063–4066.
[36] A. Togo, I. Tanaka, *Scr. Mater.* **2015**, *108*, 1–5.
[37] A. Togo, F. Oba, I. Tanaka, *Phys. Rev. B* **2008**, *78*, 134106.

Supplementary Material: The online version of this article offers supplementary material (https://doi.org/10.1515/znb-2019-0217).